3-dB Power Dividers With Equal Complex Termination Impedances and Design Methods for Controlling Isolation Circuits

Hee-Ran Ahn, *Senior Member, IEEE*, and Sangwook Nam, *Senior Member, IEEE*

***Abstract*—A 3-dB power divider (PD) terminated in equal complex impedances is presented. It consists of two identical 90° transmission-line sections and an isolation circuit, being composed of resistance and capacitance, or resistance and inductance, depending on the termination impedances. If the termination impedance has capacitance, the isolation impedance should consist of inductance, and therefore, the isolation circuit should be implemented with a chip inductor. However, the chip inductor contains additional stray capacitance and resistance, which lead to undesired frequency performance. To avoid the usage of the chip inductors, even with arbitrary termination impedances, three design methods by adding transmission-line sections, adding open stubs, and adding short stubs are introduced. The PDs designed by the three methods can have not only desired isolation impedances, but also the total size of the PDs can be reduced. To verify the suggested theory, three PDs are measured. For one PD with adding transmission-line sections, the measured reflection coefficients at all ports are −43.29, −41.55, and −51.69 dB, the isolation is 56.7 dB, and the power division is −3.042 dB at a design center frequency of 1 GHz, which agree quite well with those predicted.**

***Index Terms*—Complex termination impedances, controlling isolation circuits, impedance transformers with complex impedances, three-port 3-dB power dividers (PDs), Wilkinson PDs.**

I. Introduction

THE POWER dividers (PDs) originated from Wilkinson in 1960 [1], who described a device that separated one signal into n equiphase-equiamplitue signals. Perfect matching and perfect isolation are theoretically achieved at a design center frequency. With $n = 2$, his circuit may be reduced to a three-port 3-dB PD. Since Wilkinson, many literatures treat the PDs [2]–[10], which are used for various applications, such as antenna arrays and power amplifiers. As the wireless communication systems require substantial reduction in mass and volume, two ways for the reduction are adopted; each component itself is reduced in size [7], [9], or the total size of microwave integrated circuits are decreased by controlling the termination impedances [10]–[13] of the components. The termination impedances are, in general, of arbitrary real values, but if they are complex, the size reduction effect may be far more intensified because the input impedances of the power amplifiers or antenna arrays are not always real. For the complex termination impedances of the PDs, there is only one case [5]. Since no design formula [5] is, however, available, rigorous optimization is a unique way for the designs. Furthermore, the design processes are more complicated than required, and several stages of the PDs are needed for desired frequency performance because the isolation circuit in [5] should consist of only resistances.

In this paper, design formulas for the PD terminated in equal complex impedances are derived using complex impedance transformers with only one transmission-line section [14]. In this case, the PD consists of two identical 90° transmission-line sections and an isolation circuit. The isolation circuit depends on the termination impedances, and if the termination impedance has capacitance, the isolation impedance should be of inductance. To realize the inductance, a chip inductor is inevitably necessary. The general chip inductors, however, include stray capacitance and stray resistance, which may lead to unwanted frequency performance. To avoid the usage of the chip inductors, even with the termination impedance having capacitance, three ways to control the isolation impedances are suggested. The three are adding transmission-line sections, adding open stubs, and adding short stubs, by use of which the size reduction effect may also be expected, independent of the termination impedances.

To verify the design formulas, a PD terminated in equal complex impedances of $(41 + j10)\Omega$ designed at 1 GHz is measured. In this case, the two identical transmission-line sections are 90° long, and it would be better to reduce the 90° transmission-line sections. For this, a symmetric equivalent-circuit stepped-impedance modified Π-type (SMΠ) [15, Fig. 6(c)] is exploited. Also, to validate the methods controlling the isolation circuits, two additional PDs are constructed and measured. The measured results of the three PDs are in quite good agreement with those predicted, and the measured reflection coefficients at all ports of one PD with adding transmission-line sections are −43.29, −41.55, and −51.69 dB, the isolation is 56.7 dB, and the power division is −3.042 dB, showing the best measured performance among the three fabricated (measured) PDs.

II. Three-Port 3-dB PDs

A. Design Formulas

A PD is depicted in Fig. 1 where it is terminated in equal complex impedances of Z_L, $Z_L = R_L + jX_L$, where R_L should

Manuscript received August 06, 2013; accepted August 23, 2013. Date of publication September 25, 2013; date of current version November 01, 2013. This work was supported by the Basic Science Research Program through the National Research Foundation of Korea (NRF) funded by the Ministry of Education, Science and Technology (2009-0083495).

The authors are with the School of Electrical Engineering and Computer Science, Seoul National University, Seoul 151-742, Korea (e-mail: hranahn@gmail.com; snam@snu.ac.kr).

Color versions of one or more of the figures in this paper are available online at http://ieeexplore.ieee.org.

Digital Object Identifier 10.1109/TMTT.2013.2281101

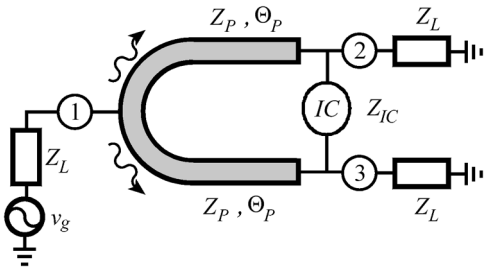

Fig. 1. PD with complex termination impedances of Z_L.

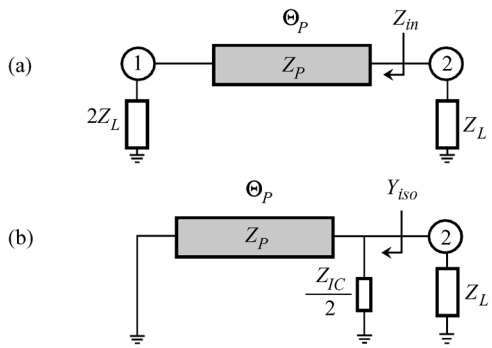

Fig. 2. (a) Even- and (b) odd-mode equivalent circuits.

TABLE I
DESIGN DATA AT 1 GHz FOR THE PDs IN FIG. 1

Z_L (Ω)	Z_P (Ω)	Z_{IC} (Ω)	C_{ap} (pF)	I_{nd} (nH)
60+*j*10	86.023	120-*j*20	7.958	
60+*j*15	87.464	120-*j*30	5.305	
60+*j*20	89.442	120-*j*40	3.979	
60-*j*10	86.023	120+*j*20		3.183
60-*j*15	87.464	120+*j*30		4.775
60-*j*20	89.442	120+*j*40		6.367

be greater than zero, while X_L is a real number including zero. The PD consists of two identical transmission-line sections with the characteristic impedance of Z_P and the electrical length of Θ_P and an isolation circuit of IC, the impedance of which is denoted as $Z_{\rm IC}$.

When the power is excited at port ① in Fig. 1, the power is divided equally into ports ② and ③, and the two ports ② and ③ are isolated by the isolation circuit. To fulfill the PD function, the values of Z_P, Θ_P, and $Z_{\rm IC}$ need to be determined. For this, the even- and odd-mode equivalent circuits are required, as depicted in Fig. 2.

The even-mode equivalent circuit in Fig. 2(a) consists of only one transmission-line section, transforming the termination impedance of $2Z_L$ into Z_L. The characteristic impedance of Z_P and the electrical length of Θ_P [14] are, therefore, obtained such as

$$Z_P = \sqrt{2}|Z_L| \tag{1a}$$

$$\Theta_P = 90^\circ \tag{1b}$$

where Θ_P may also be calculated by the perfect matching condition that $Z_{\rm in}$ in Fig. 2(a) is equal to Z_L^*, where Z_L^* is the complex conjugate of Z_L. The odd-mode equivalent circuit in Fig. 2(b) is composed of one transmission-line section (Z_p and Θ_p) and half of the isolation impedance of $Z_{\rm IC}/2$, which are connected

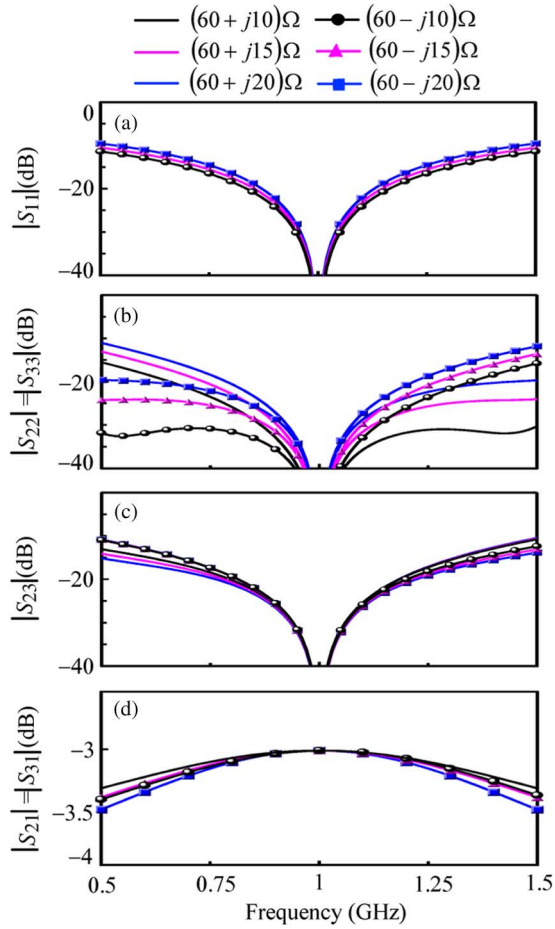

Fig. 3. Scattering parameters of the PDs. (a) $|S_{11}|$. (b) $|S_{22}| = |S_{33}|$. (c) $|S_{23}|$. (d) $|S_{21}| = |S_{31}|$.

in parallel to the termination impedance of Z_L. The input admittance looking into the isolation impedance of $Z_{\rm IC}/2$ is indicated as $Y_{\rm iso}$ in Fig. 2(b), and the relation between $Z_{\rm IC}/2$ and $Y_{\rm iso}$ is expressed as

$$Y_{\rm iso} = \frac{2}{Z_{\rm IC}} - jY_p \cot\Theta_p = \frac{1}{Z_L^*} \tag{2}$$

where $Y_p = Z_p^{-1}$.

Substituting $\Theta_P = 90^\circ$ into (2), the isolation impedance of $Z_{\rm IC}$ is computed as

$$Z_{\rm IC} = 2Z_L^*. \tag{3}$$

For the PD terminated in equal impedance of 50 Ω, the isolation impedance is 100 Ω, two identical transmission-line sections are 90° long, and the characteristic impedance is 70.7 Ω. These values can be obtained by substituting $Z_L = 50$ Ω into (1) and (3).

B. Frequency Responses

Based on the design formulas in (1)–(3), several cases with different termination impedances of Z_L were calculated in Table I, where the isolation impedances are composed of real value of $Z_{\rm IC}$ and capacitance or inductance, expressed as C_{ap} and I_{nd} at a design center frequency of 1 GHz. Their frequency responses are plotted in Fig. 3 where the scattering

parameters of $|S_{11}|$, $|S_{22}| = |S_{33}|$, $|S_{23}|$, and $|S_{21}| = |S_{31}|$ are in Fig. 3(a)–(d), respectively, under the assumption of constant termination impedances. The imaginary values of the complex termination impedances are surely frequency dependent. Nevertheless, even though it is assumed that the termination impedances are of constant complex values defined at a design center frequency, the assumption is correct, because all PDs are designed at a single frequency, and the variation behavior of the termination impedances is not easy to know.

All the PDs in Fig. 3(a) are perfectly matched at the design center frequency of 1 GHz. For the matching responses, the frequency responses with Z_L and Z_L^* are the same, and the bandwidths with $Z_L = (60 \pm j10)\Omega$ are the widest, while those with $Z_L = (60 \pm j20)\Omega$ are the smallest. For the output matching in Fig. 3(b), two responses with $Z_L = (60 \pm j10)\Omega$ are symmetric with respect to the center frequency of 1 GHz and show the widest bandwidths.

The isolation responses with $Z_L = (60 \pm j20)\Omega$ in Fig. 3(c) show the widest bandwidths, which are different from the frequency responses of $|S_{11}|$ and $|S_{22}| = |S_{33}|$. In other words, if the ratio of $|X_L|$ to R_L is the smallest, the bandwidths of the matching performance is the widest, whereas those of the isolation response is the smallest, independent of positive or negative value of X_L. All the PDs show perfect isolation performance in Fig. 3(c), and as far as the termination impedances are complex, the isolation impedance of $Z_{\rm IC}$ is also complex from (3). The power division responses in Fig. 3(d) are consistent with the matching responses in Fig. 3(a), and two cases with $X_L = \pm j15\ \Omega$ and those with $X_L = \pm j20\ \Omega$ are the same.

C. Verification of PDs

To verify the suggested theory in (1) and (3), one PD with $Z_L = (41 + j10)\Omega$ designed at 1 GHz was fabricated on a substrate (RT/Duroid 5880, $\varepsilon_r = 2.2$, $H = 0.787$ mm). In this case, each transmission-line section in Fig. 1 is 90° long, its characteristic impedance of Z_P is 59.68 Ω, and the isolation impedance of $Z_{\rm IC}$ is $(82 - j20)\Omega$, which may be realized with one chip resistor with 82 Ω and one chip capacitor with ≅8 pF at 1 GHz. Since the two identical transmission-line sections with Z_P and Θ_P are too long in a low frequency region, it would be better to make them smaller.

For this, a symmetric equivalent circuit of stepped impedance modified Π-type (SMΠ) [15, Fig. 6(c)] was employed. A 90° transmission-line section with Z_P and its equivalent circuit of SMΠ are displayed in Fig. 4. SMΠ in Fig. 4(b) consists of two identical transmission-line sections with Z_{pa} and Θ_{pa} and a modified Π-equivalent circuit [16]. The modified Π-equivalent circuit has N transmission-line sections with the characteristic impedance of Z_{sp} and $N + 1$ open stubs. The transmission-line sections and the open stubs are equally $\Theta_{\rm sp}$ and $\Theta_{o\Pi}$ long, respectively, and the characteristic impedance of the open stub is $Z_{o\Pi}$.

For the fabrication, $\Theta_{pa} = 0$, $N = 4$, and $N\Theta_{sp} = 52°$ in Fig. 4(b) were predetermined, which leads to the calculation of $Z_{sp} = 101.53\ \Omega$ and $S_\Pi^{-1} = 452.35\ \Omega$, referring to [15, eqs. (13) and (14)], where S_Π is the susceptance generated by each open stub. The fabricated PD is described in Fig. 5 where the susceptance of S_Π is realized with two different transmission-line sections with the characteristic impedances of 120 and 35 Ω. The open stub connected at the port ① is for $2S_\Pi$, which is realized with those of 120 and 30 Ω, and each S_Π at port ② or ③ is implemented with those of 120 and 40 Ω.

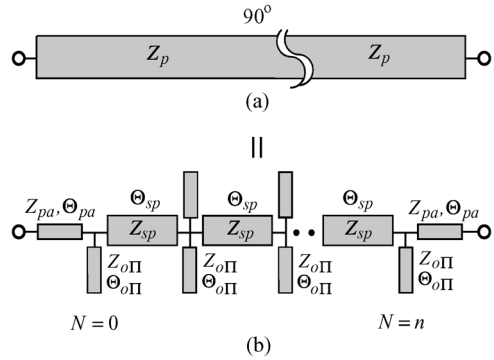

Fig. 4. (a) Transmission-line section. (b) Equivalent circuit of SMΠ.

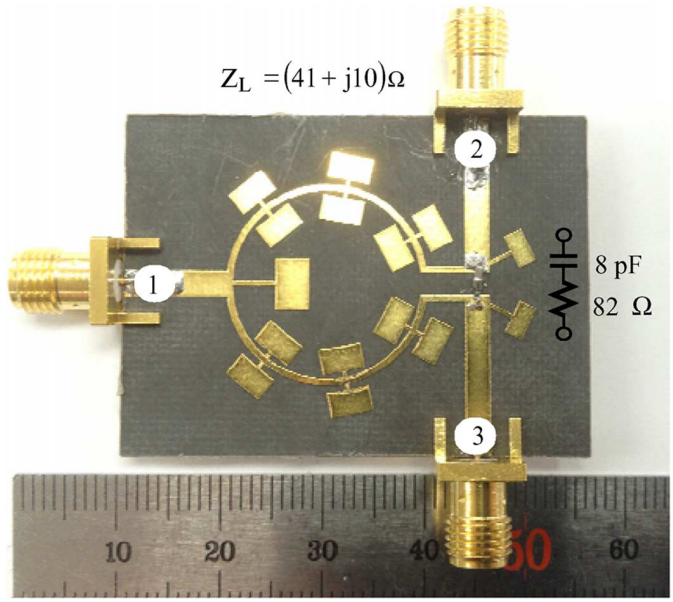

Fig. 5. Fabricated PD with $Z_L = (41 + j10)\Omega$.

The PD is terminated in equal impedance of $(41 + j10)\Omega$ and therefore no way to measure it with a 50-Ω measurement system. After measuring it with the 50-Ω termination impedances, if the measured results are converted into those with the termination impedance of $(41 + j10)\Omega$ using the Advance Design System (ADS), the converted results become the measured results with the complex termination impedances of $(41 + j10)\Omega$. The frequency responses predicted and measured are compared in Fig. 6 where input matching of $|S_{11}|$ and isolation of $|S_{23}|$ are in Fig. 6(a), the output matchings of $|S_{22}|$ and $|S_{33}|$ in Fig. 6(b), and the power divisions of $|S_{21}|$ and $|S_{31}|$ in Fig. 6(c). The measured results are in good agreement with those predicted, and the measured matching responses of $|S_{11}|$, $|S_{22}|$, and $|S_{33}|$ at 1 GHz are −29.94, −26.52, and −25.37 dB, the isolation response of $|S_{23}|$ is −29.21 dB, and the power division of $|S_{21}|$ is −3.07 dB.

III. Problems With Lumped-Element Inductors

The PDs in Fig. 1 need chip inductors or capacitors for the isolation circuits. To test whether the chip capacitors and induc-

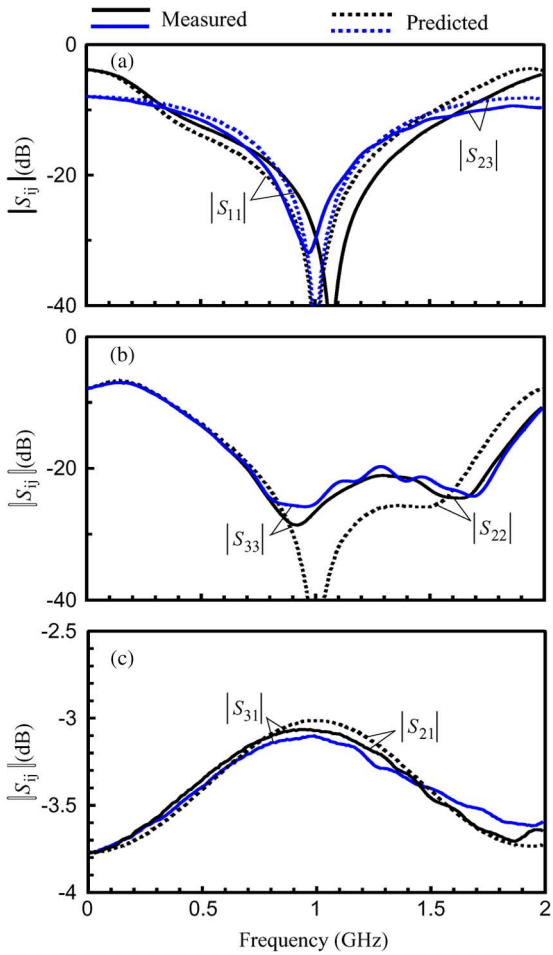

Fig. 6. Measured and predicted results. (a) $|S_{11}|$ and $|S_{23}|$. (b) $|S_{22}|$ and $|S_{33}|$. (c) $|S_{21}|$ and $|S_{31}|$.

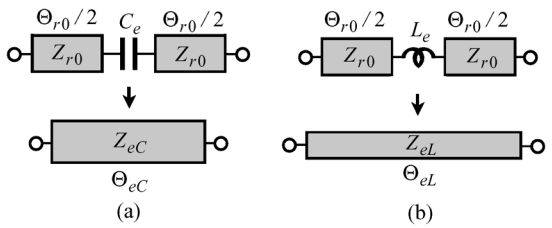

Fig. 7. Equivalent circuits. (a) Two identical transmission-line sections with a capacitance. (b) Two identical transmission-line sections with an inductance.

tors are suitable for the isolation circuits, their reliability will be examined. For this, it is necessary to understand the relations described in Fig. 7 where two identical transmission-line sections (characteristic impedance of Z_{r0} and electrical length of $\Theta_{r0}/2$) and a capacitance of C_e in Fig. 7(a) are equivalent to a transmission-line section with the characteristic impedance of Z_{eC} and the electrical length of Θ_{eC}, while those with the inductance of L_e in Fig. 7(b) are the same as that with Z_{eL} and Θ_{eL}.

The design formulas for Z_{eC}, Θ_{eC}, Z_{eL}, and Θ_{eL} in Fig. 7 are

$$Z_{eC} = Z_{r0}\sqrt{\cot\frac{\Theta_{r0}}{2}\frac{\left(Z_{r0}\tan\frac{\Theta_{r0}}{2}-\frac{1}{2\omega C_e}\right)}{Z_{r0}+\frac{1}{2\omega C_e}\tan\frac{\Theta_{r0}}{2}}} \quad (4a)$$

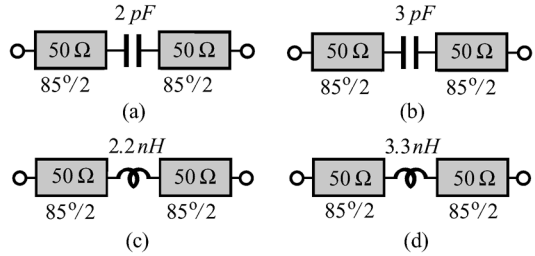

Fig. 8. Detailed circuits for measurements. (a) 2 pF. (b) 3 pF. (c) 2.2 nH. (d) 3.3 nH.

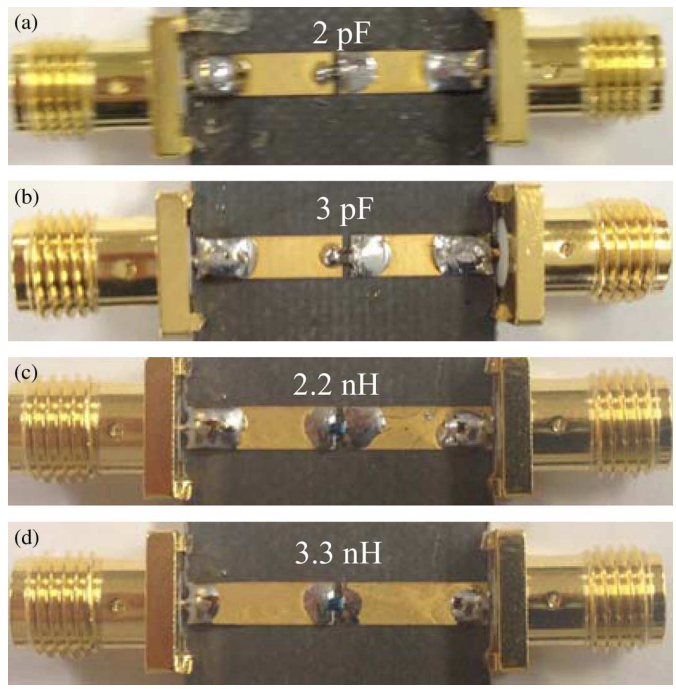

Fig. 9. Fabricated circuits for measurements. (a) 2 pF. (b) 3 pF. (c) 2.2 nH. (d) 3.3 nH.

$$\cot\frac{\Theta_{eC}}{2} = \sqrt{\cot\frac{\Theta_{r0}}{2}\frac{\left(Z_{r0}+\frac{1}{2\omega C_e}\tan\frac{\Theta_{r0}}{2}\right)}{Z_{r0}\tan\frac{\Theta_{r0}}{2}-\frac{1}{2\omega C_e}}} \quad (4b)$$

$$Z_{eL} = Z_{r0}\sqrt{\cot\frac{\Theta_{r0}}{2}\frac{\left(\frac{\omega L_e}{2}+Z_{r0}\tan\frac{\Theta_{r0}}{2}\right)}{Z_{r0}-\frac{\omega L_e}{2}\tan\frac{\Theta_{r0}}{2}}} \quad (4c)$$

$$\cot\frac{\Theta_{eL}}{2} = \sqrt{\cot\frac{\Theta_{r0}}{2}\frac{\left(Z_{r0}-\frac{\omega L_e}{2}\tan\frac{\Theta_{r0}}{2}\right)}{\frac{\omega L_e}{2}+Z_{r0}\tan\frac{\Theta_{r0}}{2}}}. \quad (4d)$$

Four measurements were carried out with four chip capacitors and inductors having 2 pF, 3 pF, 2.2 nH, and 3.3 nH, as depicted in Fig. 8. The capacitors are GRM1885series (Murata, monolithic ceramic capacitors), and the inductors are LQW15A series (Murata, SMD inductors). The reason for 2.2 and 3.3 nH is because no chip inductor with 2 and 3 nH is available. The characteristic impedance and electrical length of the identical transmission-line sections in Fig. 8 are 50 Ω and 85°/2 at a design center frequency of 3 GHz.

In those cases, the characteristic impedances of Z_{eC} with 2 and 3 pF are $Z_{eC} = 37.8017$ and 41.6677 Ω, respectively, whereas those of Z_{eL} with 2.2 and 3.3 nH are $Z_{eL} = 76.5311$ and 98.79489 Ω. That is, the circuits in Fig. 8 are not terminated

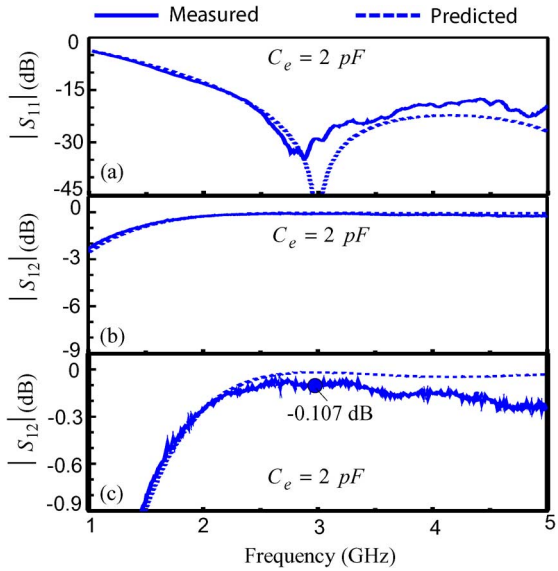

Fig. 10. Results measured and simulated are compared when 2 pF. (a) $|S_{11}|$. (b) and (c) $|S_{12}|$.

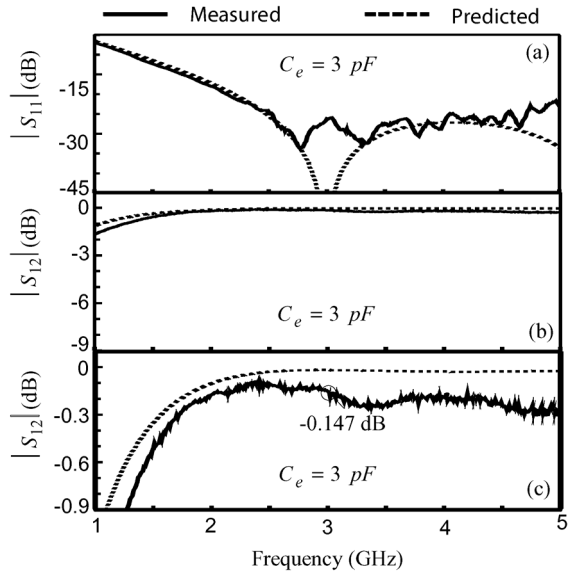

Fig. 11. Results measured and predicted are compared when 3 pF. (a) $|S_{11}|$. (b) and (c) $|S_{12}|$.

in 50 Ω. The four circuits were fabricated in Fig. 9 and measured with 50-Ω termination impedances. The measured and predicted frequency responses are, after the termination impedance compensation, compared in Figs. 10–12, where the predicted results were produced with the ideal capacitance or inductance values having no stray element. The frequency responses with 2 pF are in Fig. 10, while those with 3 pF in Fig. 11. The matching responses are in Figs. 10(a) and 11(a), while the frequency responses of $|S_{12}|$ are in Figs. 10(b) and (c) and 11(b) and (c), where additional precise insertion losses are described in Figs. 10(c) and 11(c). The measured insertion losses at the design center frequency of 3 GHz are 0.107 and 0.147 dB for 2 and 3 pF, and the bandwidths with $|S_{11}| = -15$ dB are more than 100% for both cases in Figs. 10(a) and 11(a). The measured and predicted results in Figs. 10 and 11 show quite good agreement with each other, which indicates that the chip capacitors can be used without any consideration of the stray elements.

The frequency responses for the inductors are in Fig. 12 where those of $|S_{11}|$ are in Fig. 12(a) and (c), while those of $|S_{12}|$ in Fig. 12(b) and (d). The perfect matching may occur only at the design center frequency of 3 GHz, and the insertion losses at 3 GHz are 0.282 and 0.306 dB for 2.2 and 3.3 nH, respectively. For 2.2 nH, the bandwidth with $|S_{11}| = -15$ dB is slightly more than 30% (2.4 −3.38 GHz). As shown in Fig. 12, the agreement between the measured and predicted ones is achieved only at the design center frequency of 3 GHz, and the deviation occurs even slightly outside of 3 GHz. The frequency responses of $|S_{12}|$ for the capacitors and inductors are plotted in the same scale in Figs. 10(b), 11(b), and 12(b) and (d). While quite good agreements are achieved for the capacitors, those for the inductors in Fig. 12(b) and (d) are far worse with the frequencies going higher.

From the measured results in Figs. 10–12, it can be concluded that the chip capacitors may be used with no problem of stray elements, but the utilization of the chip inductors is not desirable in terms of the stray elements and circuit theory.

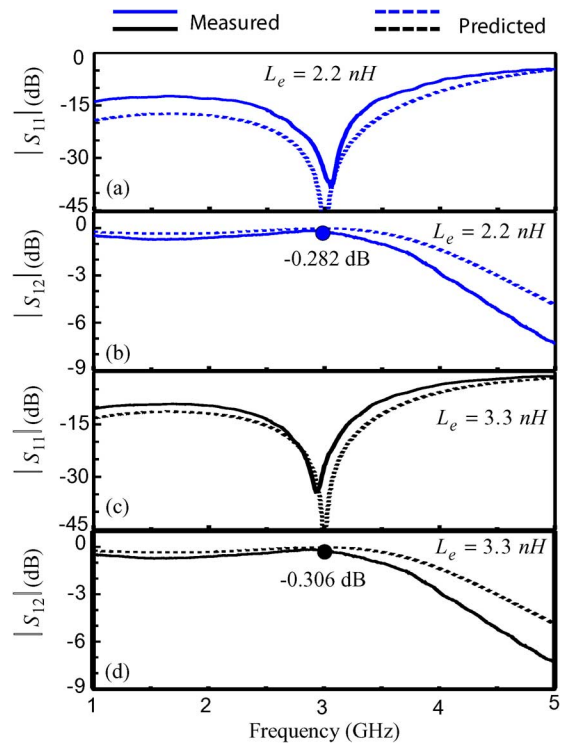

Fig. 12. Results measured and predicted are compared. (a) $|S_{11}|$ with 2.2 nH. (b) $|S_{12}|$ with 2.2 nH. (c) $|S_{11}|$ with 3.3 nH. (b) $|S_{12}|$ with 3.3 nH.

IV. Controlling Isolation Circuits

If the termination impedance of Z_L has capacitance, i.e., $X_L < 0$, the isolation circuit should be composed of resistance and inductance and fabricated with chip inductors. As demonstrated in Section III, the chip inductors, however, have loss and stray capacitance, which may cause unwanted frequency responses. To avoid employing the chip inductors even with $X_L < 0$, effective electrical length of the transmission between ports ① and ② or ports ① and ③ in Fig. 1 should be not 90°, referring to (2). For this, three methods are available, adding transmission-line sections, adding open stubs, and adding short

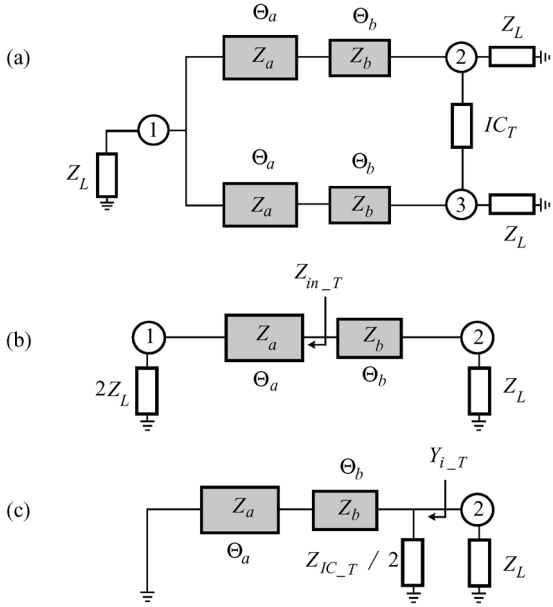

Fig. 13. (a) PD with adding transmission-line sections. (b) and (c) Its even- and odd-mode equivalent circuits.

stubs with which the circuit size of PDs can also be reduced. The methods can be applied for any termination impedance of Z_L, but will be discussed by fixing $Z_L = (65 - j10)\Omega$ to compare their isolation impedances with each other.

A. Adding Transmission-Line Sections

The resulting PD by adding the transmission-line sections is described in Fig. 13(a) where it consists of two pairs of different transmission-line sections and an isolation circuit of IC_T, being different from IC in Fig. 1. The characteristic impedances of the two different transmission-line sections are Z_a and Z_b, and the electrical lengths are Θ_a and Θ_b. Its even- and odd-mode equivalent circuits are also described in Fig. 13(b) and (c). In a similar way to the case in Fig. 2, the two transmission-line sections with Z_a and Z_b in Fig. 13(b) should be an impedance transformer to convert a complex impedance of $2Z_L$ into another one of Z_L, where the input impedance looking into the transmission-line section with Z_a is indicated as Z_{in_T}. Therefore, when a transmission-line section with Z_a and Θ_a is given in Fig. 13, the design formulas for Z_b and Θ_b are

$$Z_b = \sqrt{\frac{R_L|Z_{\mathrm{in}\_T}|^2 - Re(Z_{\mathrm{in}\_T})|Z_L|^2}{Re(Z_{\mathrm{in}\_T}) - R_L}} \tag{5a}$$

$$e^{j2\Theta_b} = \frac{\Gamma_{\mathrm{in}\_T}}{\Gamma_{L\_T}} \tag{5b}$$

where Z_b is a real value and

$$Z_{\mathrm{in}\_T} = Z_a \frac{2Z_L + jZ_a \tan\Theta_a}{Z_a + j2Z_L \tan\Theta_a} \tag{5c}$$

$$\Gamma_{\mathrm{in}\_T} = \frac{Z_{\mathrm{in}\_T} - Z_b}{Z_{\mathrm{in}\_T} + Z_b} \tag{5d}$$

$$\Gamma_{L\_T} = \frac{Z_L^* - Z_b}{Z_L^* + Z_b}. \tag{5e}$$

In the odd-mode equivalent circuit in Fig. 13(c), the input admittance looking into the half of the isolation impedance is defined as Y_{i_T} and should be equal to $(Z_L^*)^{-1}$, from which the isolation impedance of Z_{IC_T} may be found from the following relation:

$$-jY_b \frac{Y_a \cot\Theta_a - Y_b \tan\Theta_b}{Y_b + Y_a \cot\Theta_a \tan\Theta_b} + \frac{2}{Z_{\mathrm{IC}\_T}} = \frac{1}{Z_L^*} \tag{6}$$

where $Y_a = Z_a^{-1}$ and $Y_b = Z_b^{-1}$.

As far as the first term in (6) is not zero at the design frequency, $Z_{\mathrm{IC}\_T} \neq 2Z_L^*$. Thus, the isolation impedance can be controlled by choosing the appropriate value of the first term in (6). Based on (5) and (6), the isolation impedances were calculated by varying Z_a and Θ_a, and the calculation results are in Table II and Fig. 14. In this case, the termination impedance of Z_L is fixed at $(65 - j10)\Omega$.

The calculation results of Z_b and Θ_b are plotted in Fig. 14(a) and (b), while imaginary values of isolation impedances of Z_{IC_T} are in Fig. 14(c) where Z_a are varied from 20 to 100 Ω. When $Z_a = 20\ \Omega$, the maximum value of Θ_a, by which Z_b in (5a) can have real values, is around 8° in Fig. 14(a), and the lengths of Θ_b decrease with Θ_a, as displayed in Fig. 14(b). When $\Theta_a = 0°$ in Fig. 14(c), the imaginary value of Z_{IC_T} is +20 Ω due to $Z_L = (65 - j10)\Omega$. With the length of Θ_a longer than 0°, the imaginary values of Z_{IC_T} change

TABLE II
DESIGN DATA WITH $Z_L = (65 - j10)\Omega$ AND $Z_a = 40\ \Omega$ IN FIG. 13(a)

Θ_a (°)	0	4	6	8
Z_b (Ω)	93 Ω	97.91	102.65	109.95
Θ_b (°)	90.00	72.58	63.50	54.19
Z_{IC_T} (Ω)	130 +*j*20	132.9 -*j*5.1	130.6 -*j*17.9	125.98 - *j*29.9

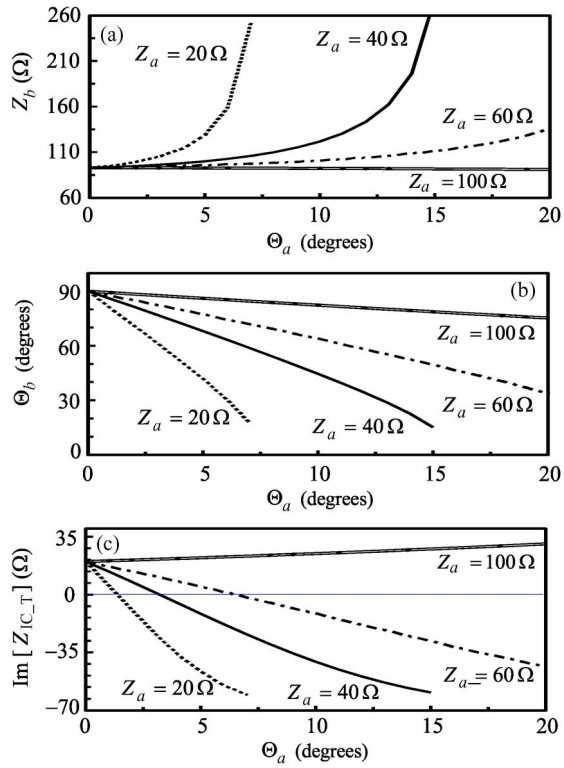

Fig. 14. Calculation results. (a) Characteristic impedances of Z_b. (b) Electrical lengths of Θ_b. (c) Imaginary values of isolation impedance of Z_{IC_T}.

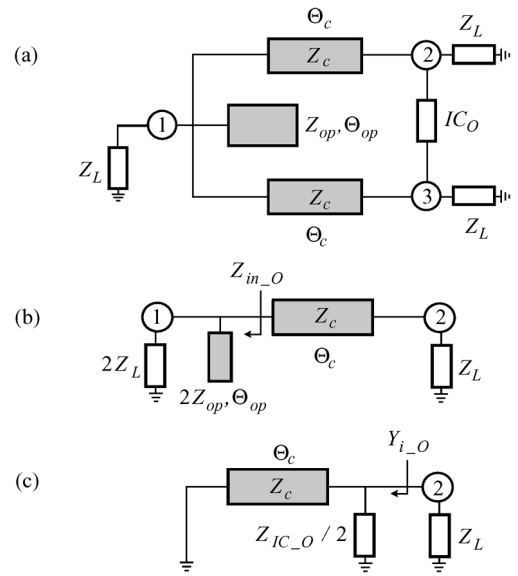

Fig. 15. (a) PD with adding an open stub. (b) (c) Its even- and odd-mode equivalent circuits.

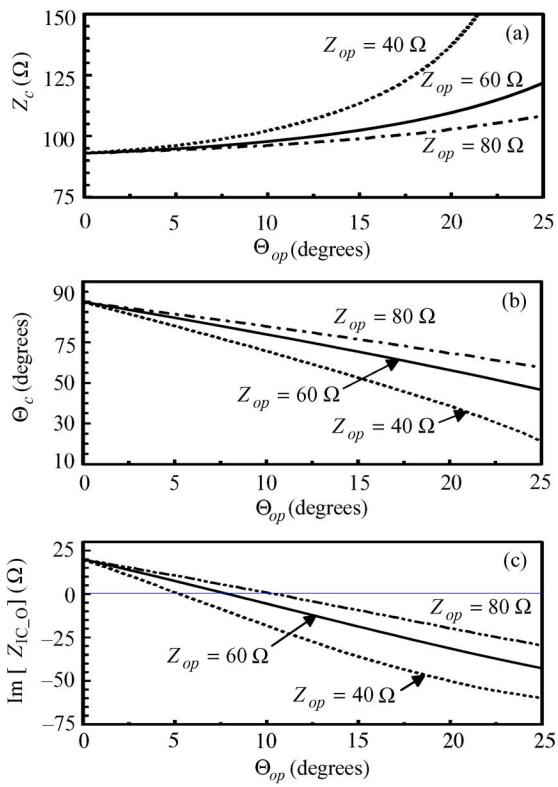

Fig. 16. Calculation results. (a) Characteristic impedances of Z_c. (b) Electrical lengths of Θ_c. (c) Imaginary values of isolation impedance of $Z_{\mathrm{IC\_O}}$.

from +20 Ω toward zero. When Θ_a reaches around 1.4° with $Z_a = 20\ \Omega$, the imaginary values of $Z_{\mathrm{IC\_T}}$ becomes zero. It indicates that Θ_a should be longer than 2°, to have negative imaginary values of $Z_{\mathrm{IC\_T}}$. When $Z_a = 40$ and 60 Ω, the variations of Z_b, Θ_b and the imaginary values of $Z_{\mathrm{IC\_T}}$ are similar to those with $Z_a = 20\ \Omega$, and Θ_a should be longer than 4° and 6°, respectively, to have negative imaginary values of $Z_{\mathrm{IC\_T}}$. When $Z_a = 100\ \Omega$, greater than $\sqrt{2}|Z_L|$ in (1a), the changes with Θ_a are quite different from those with Z_a being less than 100 Ω, and the imaginary values of $Z_{\mathrm{IC\_T}}$ are never negative. Therefore, the value of Z_a should be less than $\sqrt{2}|Z_L|$ to get the desired isolation impedance with the structure in Fig. 13(a).

B. Adding Open Stub

The first condition for the design of the PDs is that the transmission-line sections in Figs. 2(a) and 13(b) should be impedance transformer to convert $2Z_L$ into Z_L. The second condition is how to determine the isolation impedance to have capacitive isolation impedance, even with capacitive termination impedances. In other words, the second condition is to make the phase delay of the impedance transformers not ±90°, to contribute the first term in (6) to the isolation impedance. For this, the impedance transformer consisting of two transmission-line sections in Fig. 13 was treated above. Another impedance transformer to have such conditions mentioned above is to employ open stubs.

The PD with adding open stubs and its even- and odd-mode equivalent circuits are in Fig. 15, where the PD consists of two identical transmission-line sections with the characteristic impedance of Z_c and the electrical length of Θ_c, an open stub with Z_{op} and Θ_{op}, and an isolation circuit. The even- and odd-mode circuits are in Fig. 15(b) and (c) where the input impedance looking into the open stub in Fig. 15(b) is indicated as $Z_{\mathrm{in\_O}}$. The isolation circuit and isolation impedance in Fig. 15(a) and (c) are expressed as IC_O and $Z_{\mathrm{IC\_O}}$, respectively.

The design formulas for Z_c and Θ_c are, when the open stub is given, obtained such as

$$Z_c = \sqrt{\frac{R_L|Z_{\mathrm{in\_O}}|^2 - \mathrm{Re}(Z_{\mathrm{in\_O}})|Z_L|^2}{\mathrm{Re}(Z_{\mathrm{in\_O}}) - R_L}} \tag{7a}$$

$$e^{j2\Theta_c} = \frac{\Gamma_{\mathrm{in\_O}}}{\Gamma_{L\_O}} \tag{7b}$$

where Z_c is a real value and

$$Z_{\mathrm{in\_O}} = \left(\frac{1}{2Z_L} + \frac{jY_{op}\tan\Theta_{op}}{2}\right)^{-1} \tag{7c}$$

$$\Gamma_{\mathrm{in\_}o} = \frac{Z_{\mathrm{in\_O}} - Z_c}{Z_{\mathrm{in\_O}} + Z_c} \tag{7d}$$

$$\Gamma_{L\_O} = \frac{Z_L^* - Z_c}{Z_L^* + Z_c}. \tag{7e}$$

In the odd-mode circuit in Fig. 15(c), the input admittance Y_{i_O} looking into the half of the isolation impedance of $Z_{\mathrm{IC\_O}}/2$ should be equal to $(Z_L^*)^{-1}$, from which the isolation impedance of $Z_{\mathrm{IC\_O}}$ can be found from the relation

$$-jY_c\cot\Theta_c + \frac{2}{Z_{\mathrm{IC\_O}}} = \frac{1}{Z_L^*} \tag{8}$$

where $Y_c = Z_c^{-1}$.

Based on the design formulas in (7) and (8), the characteristic impedance of Z_c, the electrical length of Θ_c, and the isolation impedance of $Z_{\mathrm{IC\_O}}$ were calculated by fixing the termination impedance of $Z_L = (65 - j10)\Omega$ and varying the characteristics of the open stub, i.e., Z_{op} and Θ_{op}. The calculation results are plotted in Fig. 16, and the design data with $Z_{op} = 40\ \Omega$ are listed in Table III.

TABLE III
DESIGN DATA WITH FIXING $Z_L = (65 - j10)\Omega$ AND $Z_{op} = 40\ \Omega$ IN FIG. 15(a)

Θ_{op} (°)	4	8	12	16
Z_c (Ω)	95.3 Ω	99.4	105.9	116.8
Θ_c (°)	80.54	70.76	60.64	50.07
Z_{IC_O} (Ω)	132.9 +j5	132.2 -j10.6	128.0 -j25.6	120.5 - j38.9

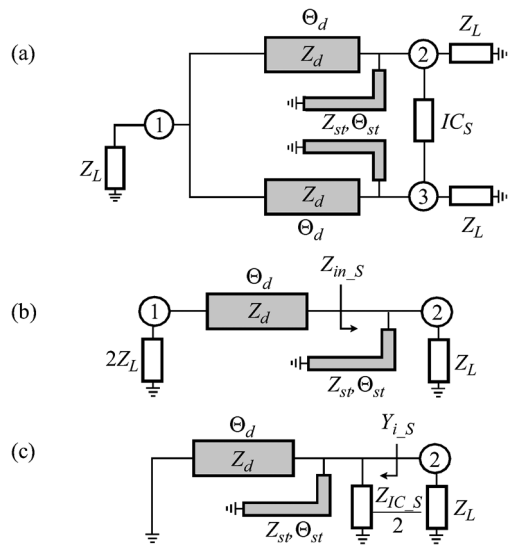

Fig. 17. (a) PD with adding short stubs. (b) and (c) Even-and odd-mode equivalent circuits.

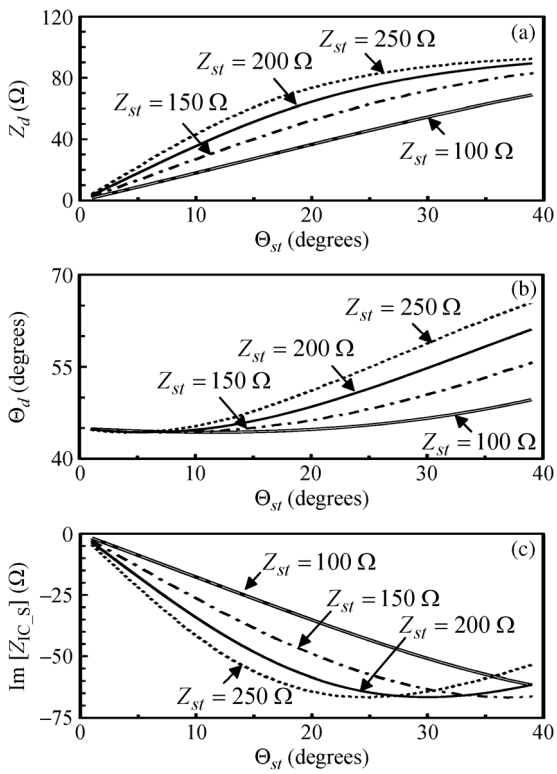

Fig. 18. Calculation results. (a) Characteristic impedance of Z_d. (b) Electrical length of Θ_d. (c) Imaginary values of isolation impedance of $Z_{\mathrm{IC\_S}}$.

When $Z_{op} = 40\ \Omega$, the maximum value of Θ_{op}, by which Z_c (7a) can have real value, is around 27° in Fig. 16(a), and the lengths of Θ_c decrease with Θ_{op}, as displayed in Fig. 16(b). When $\Theta_{op} = 0°$ in Fig. 16(c), the imaginary value of $Z_{\mathrm{IC\_O}}$ is $+20\ \Omega$ due to the termination impedance of $Z_L = (65 - j10)\Omega$. With the length of Θ_{op} longer than 0°, the imaginary values of $Z_{\mathrm{IC\_O}}$ change from $+20\ \Omega$ toward zero. When around $\Theta_{op} \cong 5.28°$ with $Z_{op} = 40\ \Omega$, the imaginary values of $Z_{\mathrm{IC\_O}}$ becomes zero. It indicates that Θ_{op} should be longer than 5.28°, to have negative imaginary values of $Z_{\mathrm{IC\_O}}$. When $Z_{op} = 60$ and $80\ \Omega$, the variations of Z_c, Θ_c and the imaginary values of $Z_{\mathrm{IC\_O}}$ are similar to those with $Z_{op} = 40\ \Omega$, and Θ_{op} should be longer than 7.9° and 10.5°, respectively, to have negative imaginary values of $Z_{\mathrm{IC\_O}}$.

C. Adding Short Stubs

The third circuit, of which the phase delay of the impedance transformer is not ±90°, is adding short stubs. The PD with the short stubs consists of two identical transmission-line sections, two identical short stubs, and an isolation circuit of IC_S, as depicted in Fig. 17(a). The characteristic impedances and the electrical lengths of the transmission-line sections and the short stubs are Z_d, Z_{st}, Θ_d, and Θ_{st}, and the isolation impedance is $Z_{\mathrm{IC\_S}}$. The even- and odd-mode equivalent circuits are in Fig. 17(b) and (c), where the input impedance looking into the short stub in Fig. 17(b) is indicated as $Z_{\mathrm{in\_S}}$.

The design formulas for Z_d and Θ_d are, when the short stub is given, obtained such as

$$Z_d = \sqrt{\frac{2R_L|Z_{\mathrm{in\_S}}|^2 - Re(Z_{\mathrm{in\_S}})|2Z_L|^2}{Re(Z_{\mathrm{in\_S}}) - 2R_L}} \tag{9a}$$

$$e^{j2\Theta_d} = \frac{\Gamma_{\mathrm{in\_S}}}{\Gamma_{L\_S}} \tag{9b}$$

where Z_d is a real value, and

$$Z_{\mathrm{in\_S}} = \left(\frac{1}{Z_L} + \frac{1}{jZ_{st}\tan\Theta_{st}}\right)^{-1} \tag{9c}$$

$$\Gamma_{\mathrm{in\_S}} = \frac{Z_{\mathrm{in\_S}} - Z_d}{Z_{\mathrm{in\_S}} + Z_d} \tag{9d}$$

$$\Gamma_{L\_S} = \frac{2Z_L^* - Z_d}{2Z_L^* + Z_d}. \tag{9e}$$

In the odd-mode equivalent circuit in Fig. 17(c), the input admittance looking into the half of the isolation impedance is Y_{i_S}, and the Y_{i_S} should be equal to $(Z_L^*)^{-1}$ for perfect matching at ports ② and ③. Thus, the following relation holds:

$$-jY_d\cot\Theta_d - jY_{st}\cot\Theta_{st} + \frac{2}{Z_{\mathrm{IC\_S}}} = \frac{1}{Z_L^*} \tag{10}$$

where $Y_d = Z_d^{-1}$ and $Y_{st} = Z_{st}^{-1}$.

Based on the design equations in (9) and (10), the characteristic impedances of Z_d, the electrical lengths of Θ_d, and the imaginary values of $Z_{\mathrm{IC\_S}}$ were calculated by varying Z_{st} and Θ_{st} under the fixed termination impedance of $Z_L = (65 - j10)\Omega$. The calculation results are plotted in Fig. 18, and the data with $\Theta_{st} = 40°$ are listed in Table IV.

The characteristic impedances of Z_d in Fig. 18(a) and the electrical lengths of Θ_d in Fig. 18(b) increase with the characteristic impedances Z_{st} and the electrical lengths Θ_{st} of the short stub, which are quite different from those of the two cases

TABLE IV
DESIGN DATA WITH FIXING $Z_L = (65 - j10)\Omega$ AND $\Theta_{st} = 40°$ IN FIG. 17(a)

Z_{st} (Ω)	100	150	200	250
Z_d (Ω)	70.27	83.92	89.96	92.73
Θ_d (°)	50.10	56.30	61.81	66.15
Z_{IC_S} (Ω)	43.62 -*j*62.4	73.27 -*j*66.2	94.48 -*j*60.38	108.11 -*j*51.95

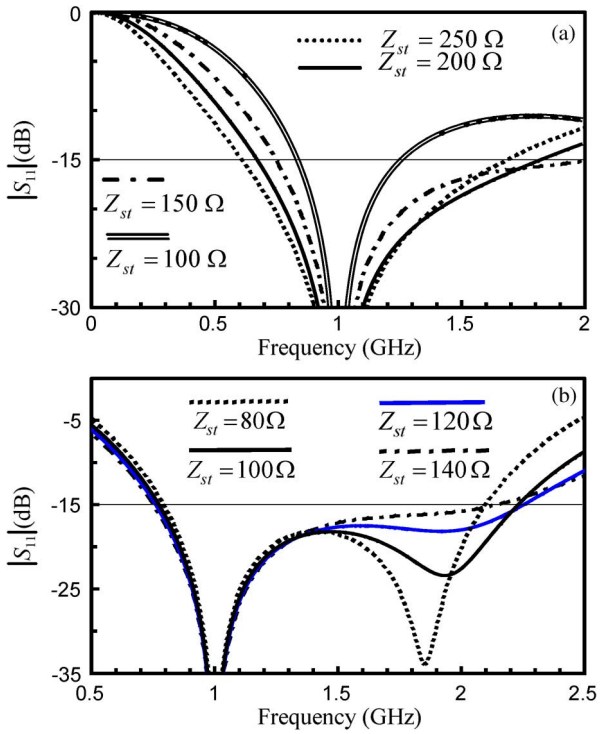

Fig. 19. Simulation results ($|S_{11}|$) of PDs with adding short stubs. (a) Fixing $\Theta_{st} = 40°$. (b) Fixing $Z_{st} \cdot \tan\Theta_{st} = 125.8\ \Omega$.

in Figs. 14 and 16. In Fig. 18(c), the imaginary values of the isolation impedance are close to zero even with the extreme short length of the short stubs and gradually become more negative with the higher characteristic impedances of Z_{st} and longer lengths of Θ_{st}, which are also quite different from those of the two cases in Figs. 14 and 16.

Even though the short stubs are of the same lengths, if the characteristic impedances of Z_{st} are different, it is natural that the design data for the PDs are different, and the frequency performance is also different. By varying Z_{st} and fixing $\Theta_{st} = 40°$, the frequency responses of the PDs are plotted in Fig. 19(a), where the bandwidth with $Z_{st} = 250\ \Omega$ is the largest, while that with $Z_{st} = 100\ \Omega$ is the smallest.

The design formulas in (9) and (10) are valid only at the design center frequency, and therefore, if the reactance value of the short stub, or, $Z_{st}\tan\Theta_{st}$ is the same, all the values for Z_d, Θ_d, and $Z_{\mathrm{IC\_S}}$ are the same. If the operating frequency is, however, outside of the center frequency, the frequency performance changes depending on the lengths of the short stubs.

With keeping $Z_{st}\tan\Theta_{st} = 125.865\ \Omega$ at 1 GHz, the electrical lengths of Θ_{st} are calculated in Table V, based on which the frequency responses are plotted in Fig. 19(b). All the responses in the frequencies lower than 1 GHz in Fig. 19(b) are about the same, and another matching frequencies, f_{other} higher than the center frequency of 1 GHz are generated. The frequencies of f_{other} are found approximately at 1.85, 2, 2.1, and 2.3 GHz for $Z_{st} = 80$, 100, 120, and 140 Ω, and higher with the higher characteristic impedances of Z_{st}. Due to the another matching frequencies, the bandwidths are also different, and the bandwidths with 15-dB return loss are 131% (0.79–2.1 GHz), 146% (0.77–2.23 GHz), 149.2% (0.76–2.252 GHz), and 140% (0.75–2.15 GHz) for $Z_{st} = 80, 100, 120$, and 140 Ω, respectively. The bandwidths may, therefore, be controlled by choosing the short stubs.

TABLE V
DESIGN DATA WITH FIXING $Z_L = (65 - j10)\Omega$ AND $Z_{st}\tan\Theta_{st} = 125.865\ \Omega$ IN FIG. 17

Z_{st} (Ω)	80 Ω	100 Ω	120 Ω	140 Ω
Z_d (Ω)	83.92	83.92	83.92	83.92
Θ_d (°)	56.3	56.3	56.3	56.3
Θ_{st} (°)	57.56	51.53	46.37	41.96

V. MEASUREMENTS

To verify the methods with which the isolation impedances can be controlled, two PDs with adding transmission-line sections and adding short stubs were fabricated on the same substrate (RT/Duroid 5880, $\varepsilon_r = 2.2$, $H = 0.787$ mm).

A. PD With Adding Transmission-Line Sections

The PD with adding transmission-line sections was fabricated at a design center frequency of 1 GHz. In this case, since the termination impedances are equally $(65 - j10)\Omega$, the isolation impedance is $(130 - j20)\Omega$, which should be implemented with a chip resistor and inductor. By adding the transmission-line sections, imaginary value of the isolation impedance changes from positive to negative. How much it changes depends on all the transmission-line sections, and available values of chip resistors and capacitors are restricted. Thus, careful choice of the two identical transmission-line sections with Z_a and Θ_a in Fig. 13 is required.

To make use of available chip resistor with 130 Ω and chip capacitor with 8 pF, the transmission-line section with Z_a and Θ_a is determined as $Z_a = 40\ \Omega$ and $\Theta_a = 6.34°$ at 1 GHz. $Z_b = 103.677\ \Omega$ and $\Theta_b = 61.938°$ are then computed. The fabricated PD with adding transmission-line sections is shown in Fig. 20, and the frequency responses measured and predicted are compared in Fig. 21 where input matching of $|S_{11}|$ and isolation of $|S_{23}|$ are in Fig. 21(a), the output matching at ports ② and ③, $|S_{22}|$, and $|S_{33}|$ are in Fig. 21(b), and the power divisions of $|S_{21}|$ and $|S_{31}|$ are in Fig. 21(c). The measured matching responses of $|S_{11}|$, $|S_{22}|$, and $|S_{33}|$ at 1 GHz are −43.29, −41.55, and −51.69 dB, the isolation response of $|S_{23}|$ is −56.7 dB, and the power division of $|S_{21}|$ is −3.042 dB, which agree quite well with those predicted.

B. PD With Adding Short Stubs

The PD with adding short stubs in Fig. 17 was fabricated at a design center frequency of 1.105 GHz. The isolation resistance is not dependent on the frequency changes, but the capacitance is dependent on the design center frequency. The center

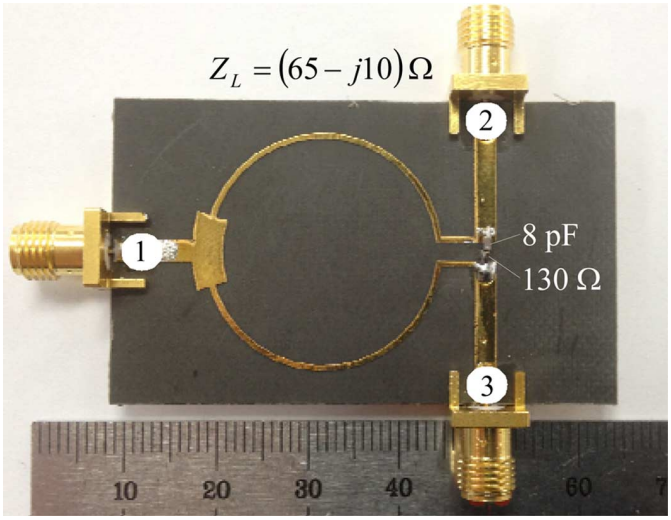

Fig. 20. Fabricated PD with adding transmission-line sections.

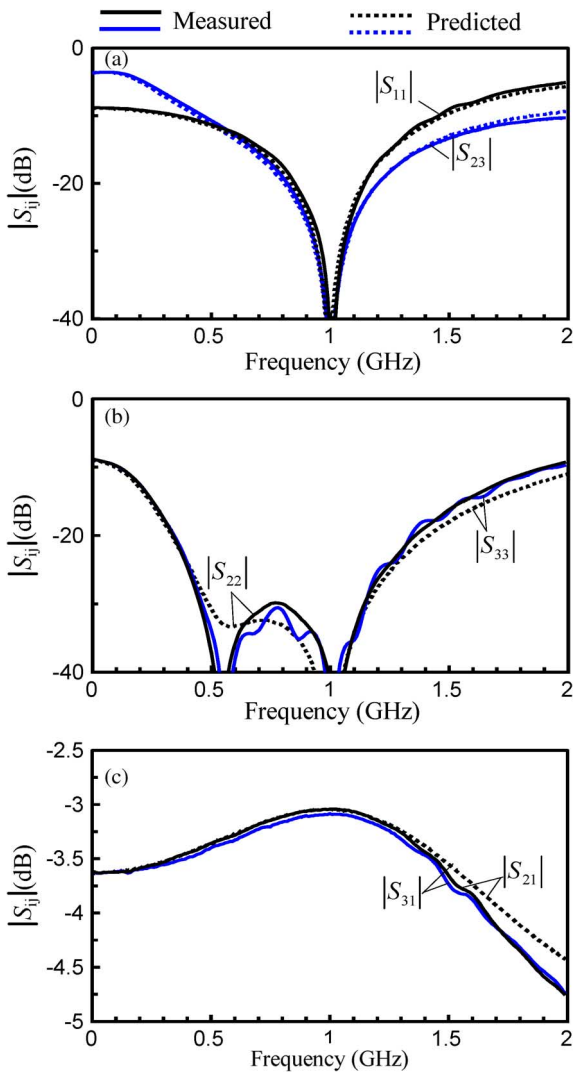

Fig. 21. Measured and predicted results of PD with adding transmission-line sections. (a) $|S_{11}|$ and $|S_{23}|$. (b) $|S_{22}|$ and $|S_{33}|$. (c) $|S_{21}|$ and $|S_{31}|$.

frequency was therefore determined so that the isolation capacitor has an available capacitance of 2.2 pF under the termination

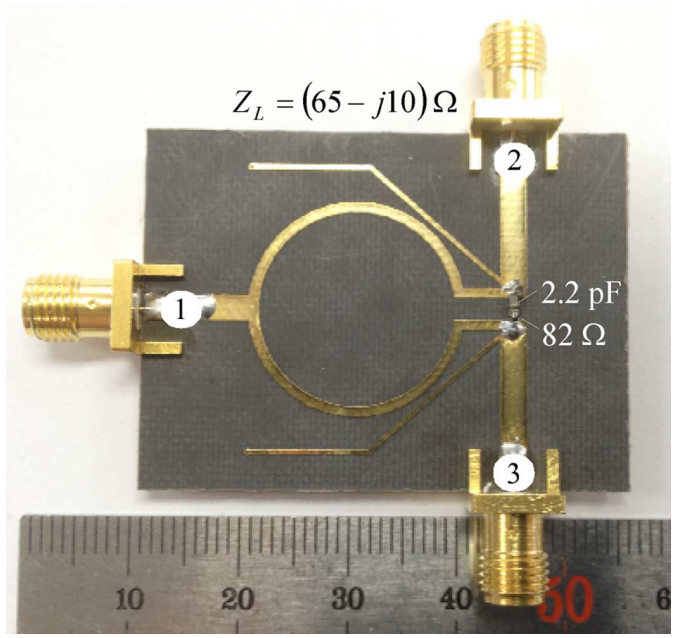

Fig. 22. Fabricated PD with adding short stubs.

impedance of $(65 - j10)\Omega$. The isolation impedance varies depending on the short stubs, which also determine the transmission-line section with Z_d and Θ_d in Fig. 17.

In this case, the short stub was chosen to have 120-Ω characteristic impedance and 49.621° electrical length. The characteristic impedance of Z_d and the electrical length of Θ_d were then calculated as 86.692 Ω and 58.43° at the design center frequency. The fabricated PD is displayed in Fig. 22 where the isolation impedance is made of a chip resistor with 82 Ω and a chip capacitor with 2.2 pF.

The frequency responses predicted and measured are compared in Fig. 23 where input matching of $|S_{11}|$ and isolation of $|S_{23}|$ are in Fig. 23(a), the output matching at ports ② and ③, $|S_{22}|$, and $|S_{33}|$ in Fig. 23(b) and the power divisions of $|S_{21}|$ and $|S_{31}|$ in Fig. 23(c). The measured matching responses of $|S_{11}|$, $|S_{22}|$, and $|S_{33}|$ at 1.105 GHz are -43.29, -28.09, and -36.07 dB, the isolation response of $|S_{23}|$ is -35.69 dB and the power division of $|S_{21}|$ is -3.041 dB, showing agreements with those predicted.

Taking account of the transmission-line sections in Figs. 20 and 22, they are each less than 90° long, which indicates that the three methods can be used not only for converting isolation circuits, but also for reducing size of the PDs with arbitrary termination impedances.

VI. Further Discussions

Letting the termination impedance of Z_L at port ① in Fig. 1 be Z_g, only the case with $Z_g = Z_L$ was investigated. In this section, why the case with $Z_g = Z_L$ is important will be further discussed. Even though any PD with $Z_g = 50\ \Omega \neq Z_L$ is desired, the PD may be designed simply by converting Z_L^* into Z_g. The ways transforming Z_L^* into $Z_g = 50\ \Omega$ are well described in [14].

For an example, if a PD with $Z_g = 50\ \Omega$ and $Z_L = (46.32 - j13.0559)\Omega$ is wanted, first consider a PD with equal termination impedances of Z_L. The PD by adding an open stub in

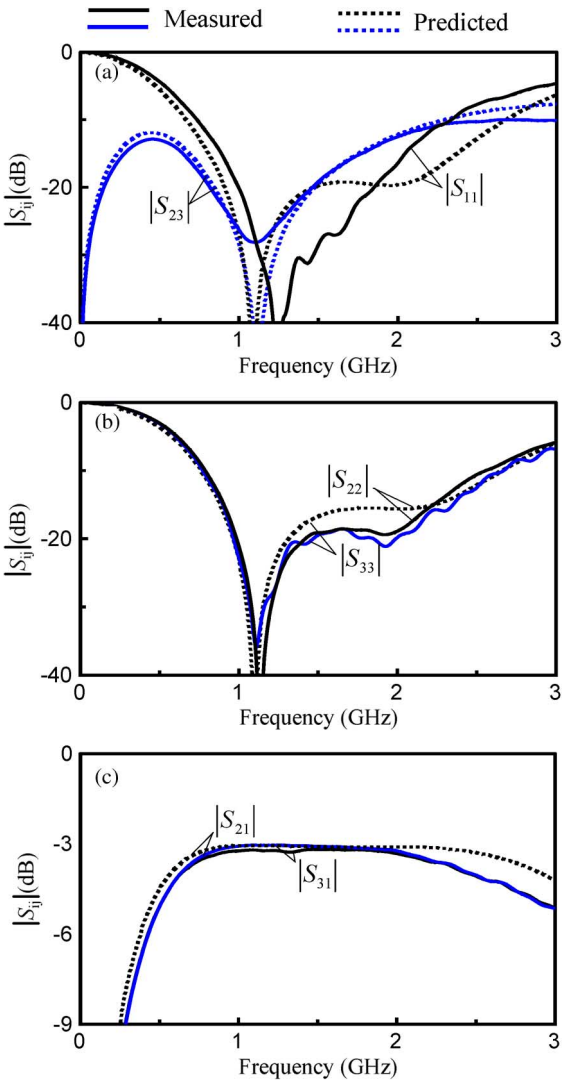

Fig. 23. Measured and predicted results of a PD with adding short stubs. (a) $|S_{11}|$ and $|S_{23}|$. (b) $|S_{22}|$ and $|S_{33}|$. (c) $|S_{21}|$ and $|S_{31}|$.

Fig. 15 is designed in Fig. 24 where the PD with equal termination impedances of Z_L is in Fig. 24(a), and the one with $Z_g = 50\ \Omega \neq Z_L$ is in Fig. 24(b) where all the calculated values may be realized with no fabrication problem. Since both PDs are designed at a center frequency of 1 GHz, all the electrical lengths are expressed as the values at 1 GHz and the capacitance value is that at 1 GHz as well.

In [5], only one case with $Z_g = 50\ \Omega$ and $Y_L = \{1/50 + j/75\tan(0.4f/f_0)\}\mho$ is treated for the PDs, where $Y_L = Z_L^{-1}$, f, and f_0 are operating and design center frequencies, respectively. When $f = f_0$, $Z_L = (46.32 - j13.0559)\Omega$, being the same as that in Fig. 24. Based on the data of the PD with $Z_g = 50\Omega$ in Fig. 24(b), two types of simulations were carried out. One is with a fixed value of Z_L defined at $f = f_0$, and another is with a frequency-dependent Z_L. The simulation results are plotted in Fig. 25 where the solid lines are the frequency responses with frequency-dependent Z_L, while dotted lines are those with the fixed value of Z_L.

In general, the bandwidths with the frequency-dependent Z_L are wider than those with the fixed Z_L, which is natural because all the elements in Fig. 24(b) are changed with frequencies as

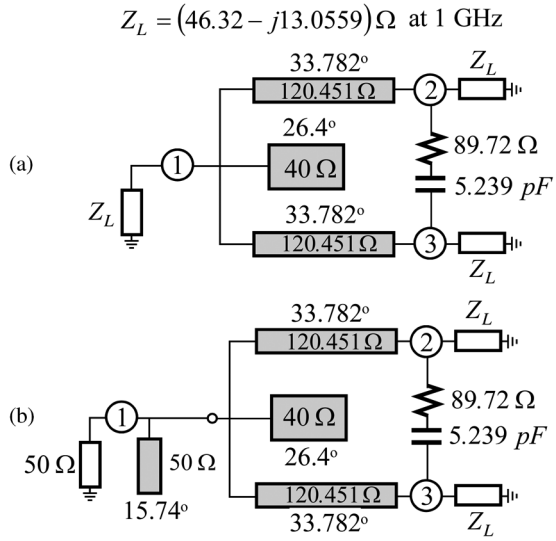

Fig. 24. Two designed PDs. (a) Equal termination impedances of Z_L. (b) $Z_g = 50\ \Omega \neq Z_L$.

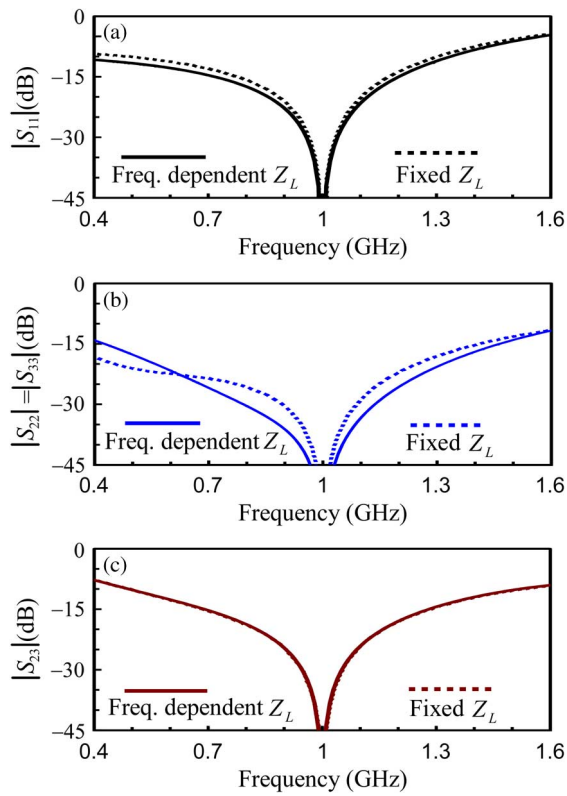

Fig. 25. Two types of simulations of the PD in Fig. 24(b). (a) $|S_{11}|$. (b) $|S_{22}| = |S_{33}|$. (c) $|S_{32}|$.

the Z_L varies with the frequencies. For the frequency-dependent Z_L, the bandwidth with 15-dB return loss at port ① is 48% (0.72–1.2 GHz), as shown in Fig. 25(a), and that at ports ② or ③ is 104% (0.43–1.470 GHz), as shown in Fig. 25(b). The isolation responses with two types in Fig. 25(c) are about the same and the bandwidth with 15-dB isolation is 59% (0.69–1.28 GHz). Perfect frequency performance of the PD is achieved at 1 GHz.

Since the open stubs in Fig. 24(b) may be replaced with the capacitors, the occupied area is mainly related with the transmission-line sections. The total transmission-line length of the PD

in Fig. 24(b) is 67.56°. On the other hand, in [5], the smallest PD has four stages and its total transmission-line length is 349.195° for a 40% bandwidth. Even worse, to design the PDs requires some time for the optimization. Therefore, it can be concluded that the design method suggested in this paper is better than the conventional one in [5], in terms of size reduction, wider bandwidths, and time saving, which is the reason for the importance of the equal complex termination impedances.

VII. Conclusions

In this paper, design formulas are derived for a PD, which can be terminated in equal complex impedances. The PD consists of two identical 90° transmission-line sections and an isolation circuit. If the termination impedance has capacitance, the isolation impedance should be of inductance and realized with a chip inductor. The chip inductor, however, not only has stray resistance, but also stray capacitance, which may introduce undesired frequency performance. To avoid the usage of the chip inductors, three methods are suggested, adding transmission-line sections, adding open stubs, and adding short stubs. To verify the suggested theory, three PDs are tested and the measured results are in good agreement with those predicted.

Since the suggested PDs may be terminated in complex impedances and may be designed with smaller size, a big advantage, that total size of integrated circuits can be reduced, may be expected in various applications of the PDs.

References

[1] E. J. Wilkinson, "An N-way hybrid power dividers," *IRE Trans. Microw. Theory Techn.*, vol. MTT-8, no. 1, pp. 116–118, Jan. 1960.

[2] Y. Sun and A. P. Freundorfer, "Broadband folded Wilkinson power combiner/splitter," *IEEE Microw. Wireless Compon. Lett.*, vol. 14, no. 6, pp. 295–297, Jun. 2004.

[3] J.-C. Kao, Z.-M. Tsai, K.-Y. Lin, and H. Wang, "A modified Wilkinson power divider with isolation bandwidth improvement," *IEEE Trans. Microw. Theory Techn.*, vol. 60, no. 9, pp. 2768–2780, Sep. 2012.

[4] L. I. Parad and R. L. Moynihan, "Split-tee power divider," *IRE Trans. Microw. Theory Techn.*, vol. MTT-8, no. 1, pp. 91–95, Jan. 1965.

[5] S. Rosloniec, "Three-port hybrid power dividers terminated in complex frequency-dependent impedances," *IEEE Trans. Microw. Theory Techn.*, vol. 44, no. 8, pp. 1490–1493, Aug. 1996.

[6] H.-R. Ahn and I. Wolff, "Three-port 3-dB power divider terminated by arbitrary impedances," in *IEEE MTT-S Int. Microw. Symp. Dig.*, 1998, pp. 781–784.

[7] H.-R. Ahn and I. Wolff, "General design equations, small-sized impedance transformers, and their application to small-sized three-port 3-dB power dividers," *IEEE Trans. Microw. Theory Techn.*, vol. 49, no. 7, pp. 1277–1288, Jul. 2001.

[8] S. Horst, R. Bairavasubramanian, M. M. Tentzeris, and J. Papapolymerou, "Modified Wilkinson power dividers for millimeter-wave integrated circuits," *IEEE Trans. Microw. Theory Techn.*, vol. 55, no. 11, pp. 2439–2446, Nov. 2007.

[9] H.-R. Ahn, "Modified asymmetric impedance transformers (MCCTs and MCVTs) and their application to impedance-transforming three-port 3-dB power dividers," *IEEE Trans. Microw. Theory Techn.*, vol. 59, no. 12, pp. 3312–3321, Dec. 2011.

[10] H.-R. Ahn and I. Wolff, "Three-port 3-dB power divider terminated by different impedances and its application to MMIC's," *IEEE Trans. Microw. Theory Techn.*, vol. 47, no. 6, pp. 786–794, Jun. 1999.

[11] H.-R. Ahn, I. Chang, and S. Yun, "Miniaturized 3-dB ring hybrid terminated by arbitrary impedances," *IEEE Trans. Microw. Theory Techn.*, vol. 42, no. 12, pp. 2216–2221, Dec. 1994.

[12] H-R. Ahn, I. Wolff, and I.-S. Chang, "Arbitrary termination impedances, arbitrary power division and small-sized ring hybrids," *IEEE Trans. Microw. Theory Techn.*, vol. 45, no. 12, pp. 2241–2247, Dec. 1997.

[13] H.-R. Ahn and I. Wolff, "Asymmetric four-port and branch-line hybrids," *IEEE Trans. Microw. Theory Techn.*, vol. 48, no. 9, pp. 1585–1588, Sep. 2000.

[14] H.-R. Ahn, "Complex impedance transformers consisting of only transmission-line sections," *IEEE Trans. Microw. Theory Techn.*, vol. 60, no. 7, pp. 2073–2084, Jul. 2012.

[15] H.-R. Ahn and S. Nam, "Compact microstrip 3-dB coupled-line ring and branch-line hybrids with new symmetric equivalent circuits," *IEEE Trans. Microw. Theory Techn.*, vol. 61, no. 3, pp. 1067–1078, Mar. 2013.

[16] H.-R. Ahn and S. Nam, "New design formulas for impedance-transforming 3-dB Marchand baluns," *IEEE Trans. Microw. Theory Techn.*, vol. 59, no. 11, pp. 2816–2823, Nov. 2011.

Hee-Ran Ahn (S'90–M'95–SM'99) received the B.S., M.S., and Ph.D. degrees in electronic engineering from Sogang University, Seoul, Korea, in 1988, 1990, and 1994, respectively.

Since April 2011, she has been with the School of Electrical Engineering and Computer Science, Seoul National University, Seoul Korea. From August 2009 to December 2010, she was with the Department of Electrical Engineering, University of California at Los Angeles, Los Angeles, CA, USA. From July 2005 to August 2009, she with the Department of Electronics and Electrical Engineering, Pohang University of Science and Technology, Pohang, Korea. From 2003 to 2005, she with the Department of Electrical Engineering and Computer Science, Korea Advanced Institute of Science and Technology, Daejeon, Korea. From 1996 to 2002, she was with the Department of Electrical Engineering, Duisburg-Essen University, Duisburg, Germany, where she was involved with the Habilitation dealing with asymmetric passive components in microwave circuits. She authored *Asymmetric Passive Component in Microwave Integrated Circuits* (Wiley, 2006). Her interests include high-frequency and microwave circuit designs and biomedical applications using microwave theory and techniques.

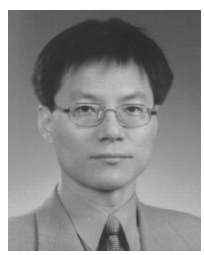

Sangwook Nam (S'87–M'88–SM'11) received the B.S. degree from Seoul National University, Seoul, Korea, in 1981, the M.S. degree from the Korea Advanced Institute of Science and Technology (KAIST), Seoul, Korea, in 1983, and the Ph.D. degree from The University of Texas at Austin, Austin, TX, USA, in 1989, all in electrical engineering.

From 1983 to 1986, he was a Researcher with the Gold Star Central Research Laboratory, Seoul, Korea. Since 1990, he has been a Professor with the School of Electrical Engineering and Computer Science, Seoul National University. His research interests include analysis/design of electromagnetic (EM) structures, antennas, and microwave active/passive circuits.